Influence of Mild Bottom Slopes on the Overtopping Flow over Mound Breakwaters under Depth-Limited Breaking Wave Conditions

Patricia Mares-Nasarre * [ID]**, M. Esther Gómez-Martín**[ID] **and Josep R. Medina**[ID]

Department of Transportation, Universitat Politècnica de València, 46022 Valencia, Spain;
mgomar00@upv.es (M.E.G.-M.); jrmedina@upv.es (J.R.M.)
* Correspondence: patmana@cam.upv.es

Abstract: The crest elevation of mound breakwaters is usually designed considering a tolerable mean wave overtopping discharge. However, pedestrian safety, characterized by the overtopping layer thickness (OLT) and the overtopping flow velocity (OFV), is becoming more relevant due to the reduction of the crest freeboards of coastal structures. Studies in the literature focusing on OLT and OFV do not consider the bottom slope effect, even if it has a remarkable impact on mound breakwater design under depth-limited breaking wave conditions. Therefore, this research focuses on the influence of the bottom slope on OLT and OFV exceeded by 2% of incoming waves, $h_{c,2\%}$ and $u_{c,2\%}$. A total of 235 2D physical tests were conducted on conventional mound breakwaters with a single-layer Cubipod® and double-layer rock and cube armors with 2% and 4% bottom slopes. Neural networks were used to determine the optimum point to estimate wave characteristics for $h_{c,2\%}$ and $u_{c,2\%}$ calculation; that point was located at a distance from the model toe of three times the water depth at the toe (h_s) of the structure. The influence of the bottom slope is studied using trained neural networks with fixed wave conditions in the wave generation zone; $h_{c,2\%}$ slightly decreases and $u_{c,2\%}$ increases as the gradient of the bottom slope increases.

Keywords: mound breakwater; overtopping; overtopping layer thickness; overtopping flow velocity; bottom slope; breaking waves

1. Introduction

Mound breakwater design criteria are evolving due to climate change effects (e.g., sea level rise) and increasing social pressure to reduce the visual impact of coastal structures. These phenomena lead to the reduction of their crest freeboards and an increase of the overtopping hazard. In this context, pedestrian safety becomes relevant due to the recreational activities that take place on the breakwater's crest (e.g., fishing and photography).

An admissible mean wave overtopping discharge, q (m³/s/m), is usually the criteria considered for design purposes. Nevertheless, Franco et al. [1] suggested that the overtopping hazard should be more directly related to individual overtopping events, rather than mean values. When assessing the overtopping hazard to pedestrians standing on coastal structures during overtopping events, several authors (see Bae et al. [2] and Sandoval and Bruce [3]) have proposed using the overtopping layer thickness (OLT) and the overtopping flow velocity (OFV) as relevant variables.

There is extensive literature on q (see EurOtop 2018 [4] and Molines and Medina [5]) and individual wave overtopping volumes (see Nørgaard et al. [6] and Molines et al. [7]) on mound breakwaters. Nevertheless, few studies have focused on OLT and OFV on dikes (see Schüttrumpf and Van Gent [8]) or on mound breakwaters (see Mares-Nasarre et al. [9]). Those studies [8,9] considered variables related

to wave characteristics and structure geometry as significant when estimating OLT and OFV. However, the bottom slope (m) has a significant influence on the type of wave breaking at the toe of the structure. Herrera et al. [10] pointed out that the bottom slope plays an important role in mound breakwater design; in depth-limited breaking-wave conditions, the optimum point where wave characteristics are estimated is relevant for design and needs to be determined.

This research focuses on the bottom slope influence on OLT and OFV during extreme overtopping events on mound breakwaters under depth-limited breaking-wave conditions. Two-dimensional physical tests were performed at the wave flume of the Universitat Politècnica de València (Spain), and data were analyzed using artificial neural networks (NNs). This paper is organized as follows. In Section 2, the variables considered in the formulas given in the literature to estimate OLT and OFV are presented. In Section 3, the experimental setup is presented. In Section 4, the analysis carried out with NNs is described; the optimum point to determine wave characteristics to estimate OLT and OFV is identified, and the bottom slope effect is assessed for both variables. Finally, in Section 5, conclusions are drawn.

2. Literature Review on Overtopping Layer Thickness (OLT) and Overtopping Flow Velocity (OFV)

Schüttrumpf and Van Gent [8] integrated the results of Van Gent [11] ($m = 1\%$ and $0.2 \leq H_s/h_s \leq 1.4$, H_s being the significant wave height at the toe of the structure and h_s the water depth at the toe) and Schüttrumpf et al. [12] (horizontal bottom and $0.1 \leq H_s/h_s \leq 0.3$) and described the overtopping flow on dike crests using two variables: (1) the OLT on the dike crest exceeded by 2% of the incoming waves, $h_{c,2\%}$, and (2) the OFV on the dike crest exceeded by 2% of the incoming waves, $u_{c,2\%}$. These authors also proposed a method to estimate $h_{c,2\%}$ and $u_{c,2\%}$ based on the wave run-up height exceeded by 2% of the incoming waves, $Ru_{2\%}$, obtained with the formulas proposed by Van Gent [13]. Van Gent [13] considered $Ru_{2\%}$ as a function of the surf similarity parameter or Iribarren number, $\xi_{s,-1}$, calculated with H_s and the spectral period $T_{m-1,0} = m_{-1}/m_0$, where m_i is the i-th spectral moment, and $m_i = \int_0^\infty S(f) f^i \, df$, being the wave spectrum $S(f)$. Following the Schüttrumpf and Van Gent [8] method, once $Ru_{2\%}$ is estimated, OLT and OFV on the seaward edge of the dike crest can be obtained: $h_{A,2\%}(R_c) = h_A(z_A = R_c)$ and $u_{A,2\%}(R_c) = u_A(z_A = R_c)$. Figure 1 shows the variables considered in the model proposed by the aforementioned authors, where MWL is the mean water level.
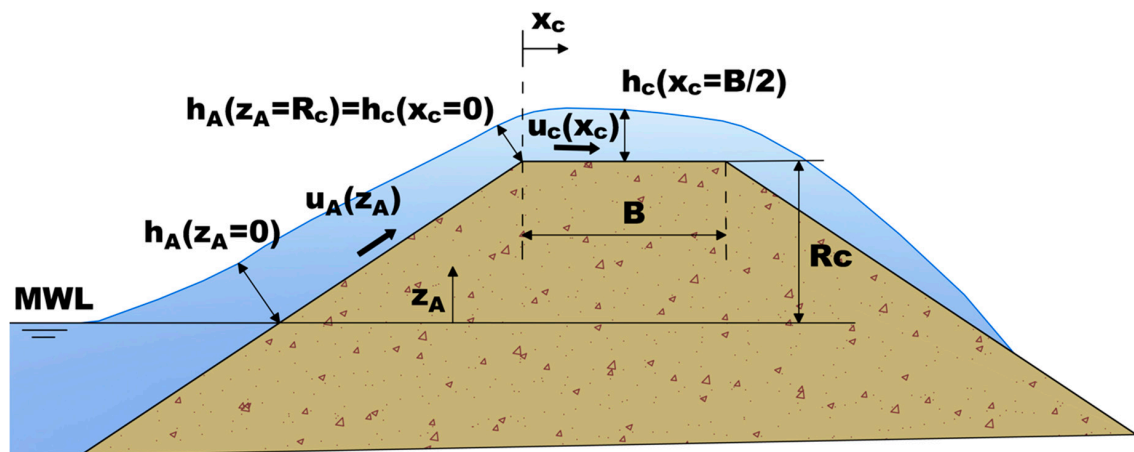
Figure 1. Definition of the variables considered by Schüttrumpf and Van Gent [8] to estimate overtopping layer thickness (OLT) and overtopping flow velocity (OFV) on a dike.

The OLT and OFV along the seaward slope of the dike depend on the $Ru_{2\%}$ calculated using the formula by Van Gent [13], the elevation over the MWL, z_A, and the significant wave height at the toe of the structure, H_s.

Using the previously calculated values of $h_{A,2\%}(z_A = R_c)$ and $u_{A,2\%}(z_A = R_c)$, OLT and OFV on the crest of the dike, $h_{c,2\%}$ and $u_{c,2\%}$, are estimated using the distance from the intersection between the seaward slope and the crest, x_c, the crest width, B, and a friction coefficient, μ (see [12] for further guidance on this coefficient).

Van der Meer et al. [14] added their new test observations on dikes (using an overtopping simulator) to the data obtained by Schüttrumpf and Van Gent [8]. Based on the new dataset, Van der Meer et al. [14] proposed a new method to estimate OLT and OFV on dikes; $h_{A,2\%}$ and $u_{A,2\%}$ estimators considered the same variables as Schüttrumpf and Van Gent [8]. The $u_{c,2\%}$ formula included the wavelength based on the spectral period ($T_{m-1,0}$), $L_{m-1,0}$.

Lorke et al. [15] carried out physical model tests on dikes (horizontal bottom and $0.1 \leq H_s/h_s \leq 0.3$) focused on the effect of currents and wind on overtopping. Using this dataset, the authors proposed new empirical coefficients for the $h_{c,2\%}$ formulas obtained by Schüttrumpf and Van Gent [8] as a function of the seaward slope of the dike, α.

EurOtop [4] recommended a new method to estimate OLT and OFV on dikes. The formulas to estimate OLT and OFV along the seaward slope are equivalent to those proposed by Schüttrumpf and Van Gent [8] but consider different empirical coefficients. As Lorke et al. [15], EurOtop [4] considers these empirical coefficients as a function of the seaward slope of the dike, α. Regarding $u_{c,2\%}$, EurOtop [4] suggests the formula given by Van der Meer et al. [14].

Mares-Nasarre et al. [9] adapted the formulas given by Schüttrumpf and Van Gent [8] to estimate $h_{c,2\%}(x_c = B/2)$ on mound breakwaters with $m = 2\%$ and $0.2 \leq H_s/h_s \leq 0.7$. These authors proposed new empirical coefficients and roughness factors for three armor layers (Cubipod®-1Layer, randomly placed cube-2Layers, and rock-2Layers). Mound breakwaters (permeable structures) and dikes are different structures, but $h_{c,2\%}(x_c = B/2)$ seems to be related to the same variables. Regarding $u_{c,2\%}(x_c = B/2)$, it is calculated as a function of the squared root of $h_{c,2\%}(x_c = B/2)$.

Table 1 summarizes the variables considered in the models proposed by the aforementioned authors to estimate $h_{c,2\%}$ and $u_{c,2\%}$.

Table 1. Summary of the variables considered for the estimation of OLT and OFV in the literature.

	Author	H_s	$T_{m-1,0}$	α	R_c	B	μ	$L_{m-1,0}$	m
$h_{A,2\%}$	Schüttrumpf and Van Gent [8]	x	x	x					
	Van der Meer et al. [14]	x	x	x					
	EurOtop [8]	x	x	x					
$u_{A,2\%}$	Schüttrumpf and Van Gent [8]	x	x	x					
	Van der Meer et al. [14]	x	x	x					
	EurOtop [8]	x	x	x					
$h_{c,2\%}$	Schüttrumpf and Van Gent [8]	x	x	x	x	x			
	Lorke et al. [15]	x	x	x	x				
	EurOtop [8]	x	x	x	x				
	Mares-Nasarre et al. [9]	x	x	x	x	x			
$u_{c,2\%}$	Schüttrumpf and Van Gent [8]	x	x	x	x		x		
	Van der Meer et al. [14]	x	x	x	x			x	
	EurOtop [8]	x	x	x	x			x	
	Mares-Nasarre et al. [9]	x	x	x	x	x			

It can be concluded from Table 1 that only geometric variables of the coastal structure and wave characteristics at the structure toe were considered in the formulations given in the literature to estimate $h_{c,2\%}$ and $u_{c,2\%}$. Even if Van Gent [11], Schüttrumpf and Van Gent [8], and van der Meer et al. [14] were considering physical tests under depth-limited breaking-wave conditions, none of them considered the bottom slope (m) as a significant variable or analyzed the optimum point for measuring wave characteristics. Here, the optimum point to estimate incident wave characteristics is considered to be the point where the error in the estimation of OLT and OFV is lowest.

3. Experimental Methodology

Two-dimensional small-scale physical tests were carried out in the wave flume (30 m × 1.2 m × 1.2 m) of the Laboratory of Ports and Coasts at the Universitat Politècnica de València (LPC-UPV), with a piston-type wave maker and two bottom slope (*m*) configurations. The first configuration corresponded to a continuous ramp of *m* = 4% all along the flume. The second configuration was composed by two ramps: one 6.3 m long and of which *m* = 4%, and one 9.0 m long and of which *m* = 2%. Figure 2 presents the longitudinal cross-sections of the LPC-UPV wave flume configurations as well as the location of the free surface wave gauges.
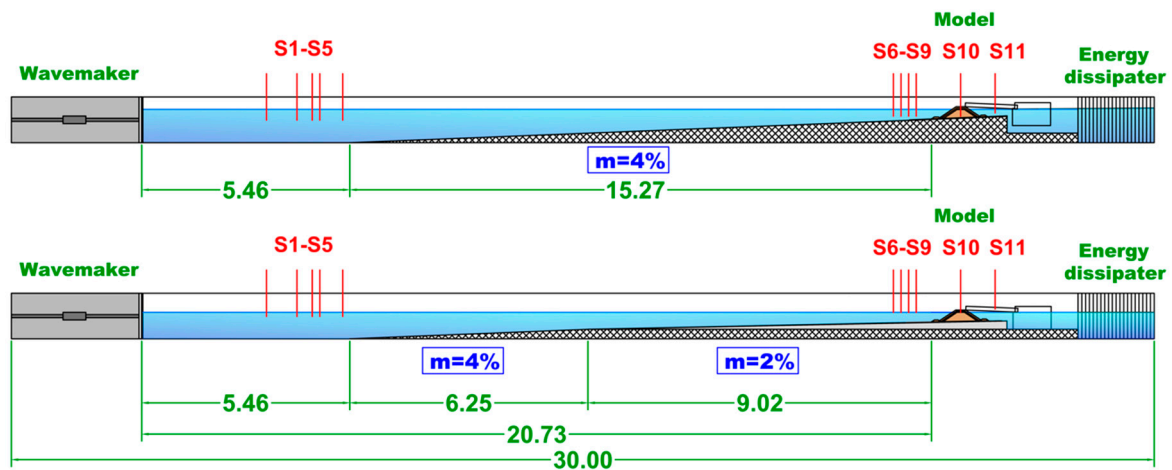
Figure 2. Longitudinal cross section of the Laboratory of Ports and Coasts at the Universitat Politècnica de València (LPC-UPV) wave flume. Dimensions are in meters.

The tested cross section depicted in Figure 3 corresponds to a mound breakwater with a cotα = 1.5 slope and rock toe berms. Three armor layers were tested: a single-layer Cubipod® armor, a double-layer randomly placed cube armor, and a double-layer rock armor. The nominal diameters or equivalent cube sizes were Dn = 3.79 cm (Cubipod®-1L), Dn = 3.97 cm (cube-2L), and Dn = 3.18 cm (rock-2L). The rock toe berm was designed to guarantee its stability. Thus, tests in which *m* = 2% were performed with a medium-sized rock toe berm (Dn_{50} = 2.6 cm), while tests in which *m* = 4% were conducted with a larger rock toe berm (Dn_{50} = 3.9 cm).
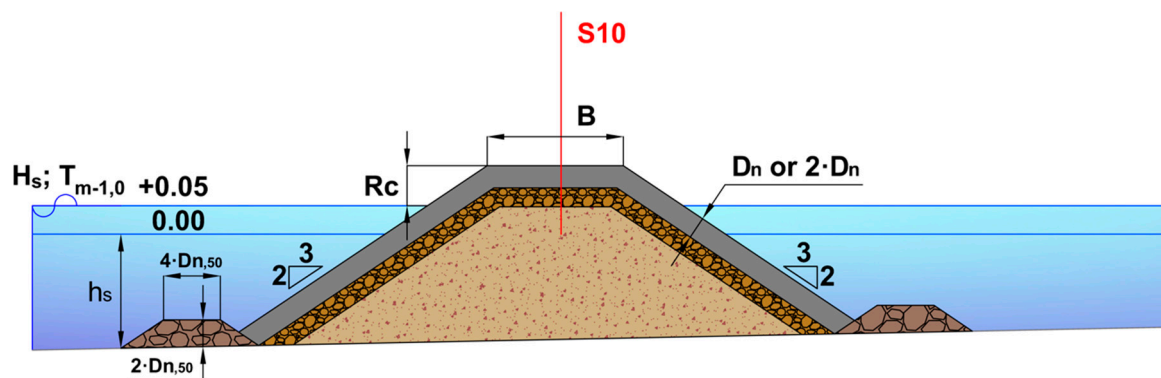
Figure 3. Cross section of the tested models in the LPC-UPV wave flume (dimensions in meters).

Two water depths (h_s) at the toe of the structure were tested for each mound breakwater model on every foreshore configuration. In the tests for which *m* = 4%, h_s equaled either 20 or 25 cm. For the tests with the Cubipod® and rock armored models, when *m* = 2%, h_s was either 20 or 25 cm. For the tests with the cube armored model, when *m* = 2%, h_s equaled either 25 or 30 cm.

For each h_s, the significant wave height ($H_s = 4(m_0)^{0.5}$) and peak period (T_p) at the wave generation zone were calculated so as to keep the Iribarren number approximately constant along the test series ($Ir_p = \tan \alpha/[2 \pi H_s/(g T_p^2)]^{0.5}$). For each Ir_p, H_s at the generation zone (H_{sg}) was increased in steps of 1 cm from no damage until the armor layer failed or waves broke at the wave generation zone.

One thousand irregular waves were generated during each test following a JONSWAP spectrum ($\gamma = 3.3$). Thus, the tests lasted approximately 15 to 35 min, depending on the mean wave period. The AWACS (Active Wave Absorption Control System) system was activated to avoid multireflections. Neither low-frequency oscillations nor piling-up (wave gauge S11) were significant during the tests.

As explained in Mares-Nasarre et al. [9], two corrections were applied to the crest freeboard because of its impact on wave overtopping: (1) the extracted accumulated overtopping volumes during a working day, and (2) the natural evaporation and facility leakages. These corrections produced a small increase in the considered crest freeboard over time on the order of 10 mm for a long working day (a 3.9% variation in terms of water depth). The crest freeboard obtained after the two previous considerations is the one applied in the following analysis. A summary of the geometry and wave characteristics in the test is presented in Table 2.

Table 2. Summary of geometry and wave characteristics in the LPC-UPV tests.

Armor	m [–]	R_c [m]	B [m]	h_s [m]	H_s [m]	T_p [s]	$T_{m-1,0}$ [s]	# Tests
Cubipod®—1L	2%	0.07–0.12	0.24	0.20 and 0.25	0.06–0.18	1.25–2.68	1.03–2.24	53
	4%	0.07–0.12		0.20 and 0.25	0.07–0.18	1.12–2.69	1.03–2.21	49
Cube—2L	2%	0.08–0.17	0.27	0.25 and 0.30	0.06–0.18	1.00–2.68	0.91–2.25	49
	4%	0.06–0.12		0.20 and 0.25	0.09–0.17	1.25–2.69	1.17–2.33	44
Rock—2L	2%	0.10–0.15	0.26	0.20 and 0.25	0.07–0.13	1.12–2.15	0.99–1.88	21
	4%	0.10–0.15		0.20 and 0.25	0.09–0.14	1.25–2.40	1.19–2.06	19

A total of 11 capacitive wave gauges were located along the flume to measure the water surface elevation (see Figure 2). Wave gauges S1–S5 were placed in the wave generation zone following Mansard and Funke [16] recommendations, while wave gauges S6–S9 were placed close to the model. In order to minimize the error in the separation of incident and reflected waves, Mansard and Funke [16] proposed several criteria to calculate the distance between wave gauges as a function of the wavelength in order to separate incident and reflected waves. Nevertheless, methods in the literature to separate incident and reflected waves are not reliable in breaking conditions. Thus, in the model zone where depth-limited breaking takes place, they are not applicable. The distances from S6–S9 to the model toe were a function of the water depth at the toe of the structure, h_s. S6, S7, S8, and S9 were placed at distances $5h_s$, $4h_s$, $3h_s$ and $2h_s$ from the toe of the model, respectively, following the recommendations given by Herrera and Medina [17]. Wave gauge S10 was located in the middle of the model crest, and S11 was located behind the model.

The experimental set up also included three cameras to analyze the armor damage in the frontal slope, on the crest, and at the rare side of the armor using the virtual net method [18] as explained in Argente et al. [19] and Gómez-Martín et al. [20]. Overtopping discharges were collected and measured using a collection tank and a weighing system behind the model during each test.

3.1. Wave Analysis

Waves were analyzed following the methodology for depth-limited breaking waves proposed by Herrera and Medina [17] and Herrera et al. [10], and similar validations to those proposed by the authors were conducted. Note that this methodology is applicable when reflection is relevant but not dominant (reflection coefficient $K_r = H_{s,r}/H_{s,i} < 0.4$, where $H_{s,r}$ and $H_{s,i}$ are the reflected and incident spectral significant wave height, respectively). Figure 4 shows the reflection coefficients measured in the wave generation zone as a function of the wave number ($k = 2\pi/L_{m0}$, where L_{m0} is the mean deep waters wavelength, obtained from the spectral mean wave period, $T_{01} = m_0/m_1$).
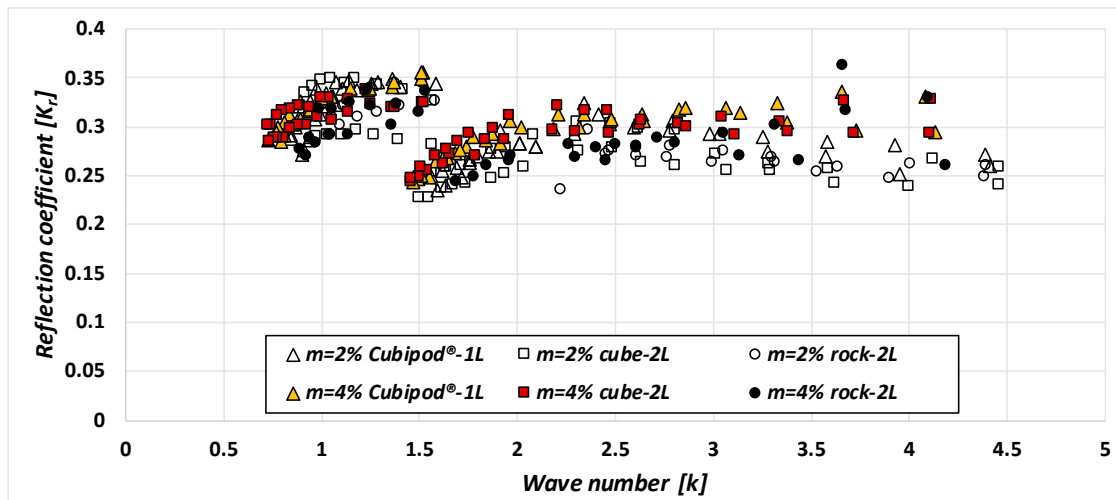
Figure 4. Reflection coefficient, K_r, as a function of the wave number, k.

The LASA-V method [21] (Local Approximation using Simulated Annealing) was applied in the wave generation zone to separate incident and reflected waves using wave gauges S1–S5. Although the LASA-V method is applicable to nonlinear and nonstationary irregular waves, it is not valid for breaking waves. Thus, it is not applicable in the model zone where breaking occurs, as is the case with other existing methods in the literature. Incident waves were estimated in the model zone from the total wave gauge records, considering the reflection coefficient ($K_r = H_{s,r}/H_{s,i} < 0.4$, $H_{s,r}$ and $H_{s,i}$ being the reflected and incident spectral significant wave height, respectively) measured in the wave generation zone. Tests without a structure were conducted in this study using an efficient wave absorption assembly located at the end of the flume ($K_r < 0.25$ measured in the wave generation zone). Thus, the measured waves directly corresponded to the incident waves. Figure 5a compares the incident significant wave height in the model zone from the tests conducted with a structure (assuming the measured K_r in the generation zone as constant) and the incident significant wave height in the model zone from the tests without a structure. To quantify the goodness of fit, the relative mean squared error (*rMSE*) and the correlation coefficient (*r*) were used. The proportion of the variance not explained by the model is estimated by $0\% < rMSE < 100\%$, whereas $0 < r < 1$ assesses the correlation between the variables. Thus, the lower the *rMSE* is and the higher *r* is, the better the estimation. *rMSE* and *r* are given by Equations (1) and (2), respectively,

$$rMSE = \frac{MSE}{var} = \frac{\frac{1}{N_o}\sum_{i=1}^{N_o}(o_i - e_i)^2}{\frac{1}{N_o}\sum_{i=1}^{N_o}(o_i - \overline{o})^2} \tag{1}$$

$$r = \frac{\sum_{i=1}^{N_o}(o_i - \overline{o})(e_i - \overline{e})}{\sqrt{\sum_{i=1}^{N_o}(o_i - \overline{o})^2 \sum_{i=1}^{N_o}(e_i - \overline{e})^2}} \tag{2}$$

where *MSE* is the mean squared error, *var* is the variance of the observations, N_o is the number of observations, o_i is the observed value, e_i is the estimation value, $\overline{o}$ is the average of the observations, and $\overline{e}$ is the average of the estimations.
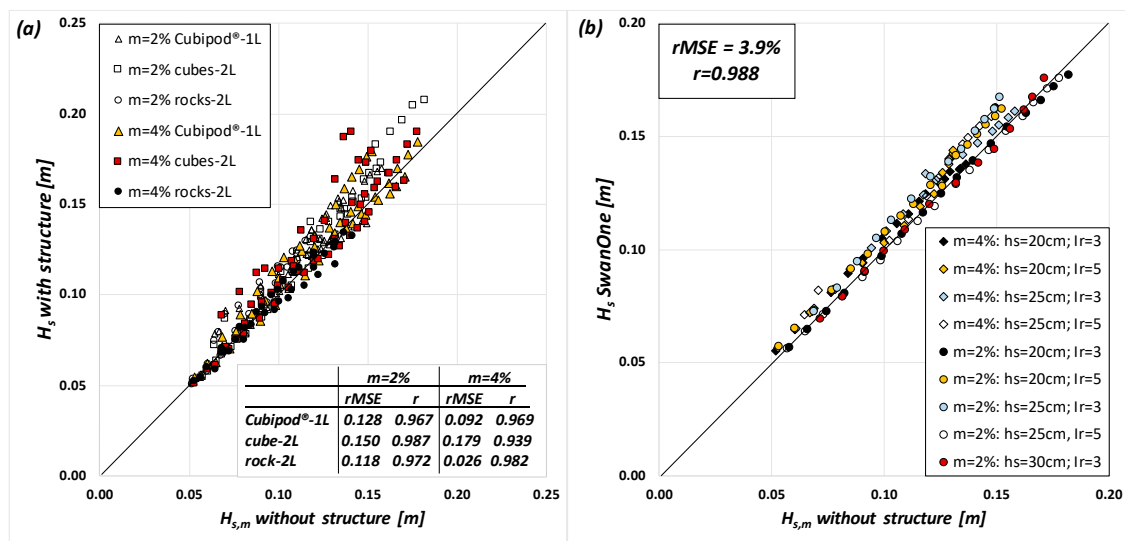
Figure 5. Comparison of the measured significant wave height in the model zone from the tests without a structure with (**a**) the incident significant wave height in the model zone from the tests conducted with a structure using K_r and (**b**) the incident wave height obtained using SwanOne.

As shown in Figure 5a, a high correlation was found between the incident wave heights obtained from tests with and without a structure. Therefore, when reflection is small ($K_r < 0.4$), the incident significant wave height obtained from the K_r measured in the wave generation zone is a good estimator of the actual incident significant wave height. This result agrees with those reported in [10] and [17]. However, as those authors [17] pointed out, measurements without a structure are more reliable when estimating incident waves, and they were the ones used for the following analysis.

The composite Weibull distribution suggested by Battjes and Groenendijk [22] to describe the wave height distribution in shallow foreshores has been widely validated in the studies of mound breakwaters in depth-limited breaking-wave conditions (i.e., [6] or [23]). This distribution was implemented in the SwanOne software [24], which was proposed by Herrera and Medina [17] as an alternative for tests conducted without a structure. Herrera and Medina [17] applied the SwanOne model to estimate the incident wave height in the model zone by introducing the incident waves at the wave generation zone. They validated this methodology comparing the measurements in the wave flume without a structure with the results from the numerical SwanOne simulations. A similar comparison was conducted in this study and it is presented in Figure 5b. A high correlation was found between the experimental measurements and the predictions given by the SwanOne model ($rMSE = 3.9\%$, $r = 0.988$). Thus, the SwanOne model is a very good estimator of the actual incident significant wave height. Since the SwanOne model provided better results than those obtained from the experimental measurements with a structure, the SwanOne predictions were used for the following analysis.

3.2. Overtopping Layer Thickness (OLT) and Overtopping Flow Velocity (OFV) Measurement

As shown in Figure 2, the capacitive wave gauge S10 was located in the middle of the breakwater crest to measure OLT. S10 was introduced into a hollow cylinder inserted in the model; S10 was filled up with water, so as to keep the capacitive wave gauge partially submerged. In order to keep the daily calibrated reference level constant, the upper part of the cylinder was closed using a lid with a slot to pass the wave gauge. The cylinder was 85 mm in diameter and 120 mm in length. Visual inspection showed a clear water surface during the overtopping events, so aeration was considered negligible. Low noise and low variation in the reference level were observed; the performance of S10 was excellent. In this study, the maximum measured OLT during each overtopping event was considered the observed $h_c(B/2)$, as shown in Figure 6a.
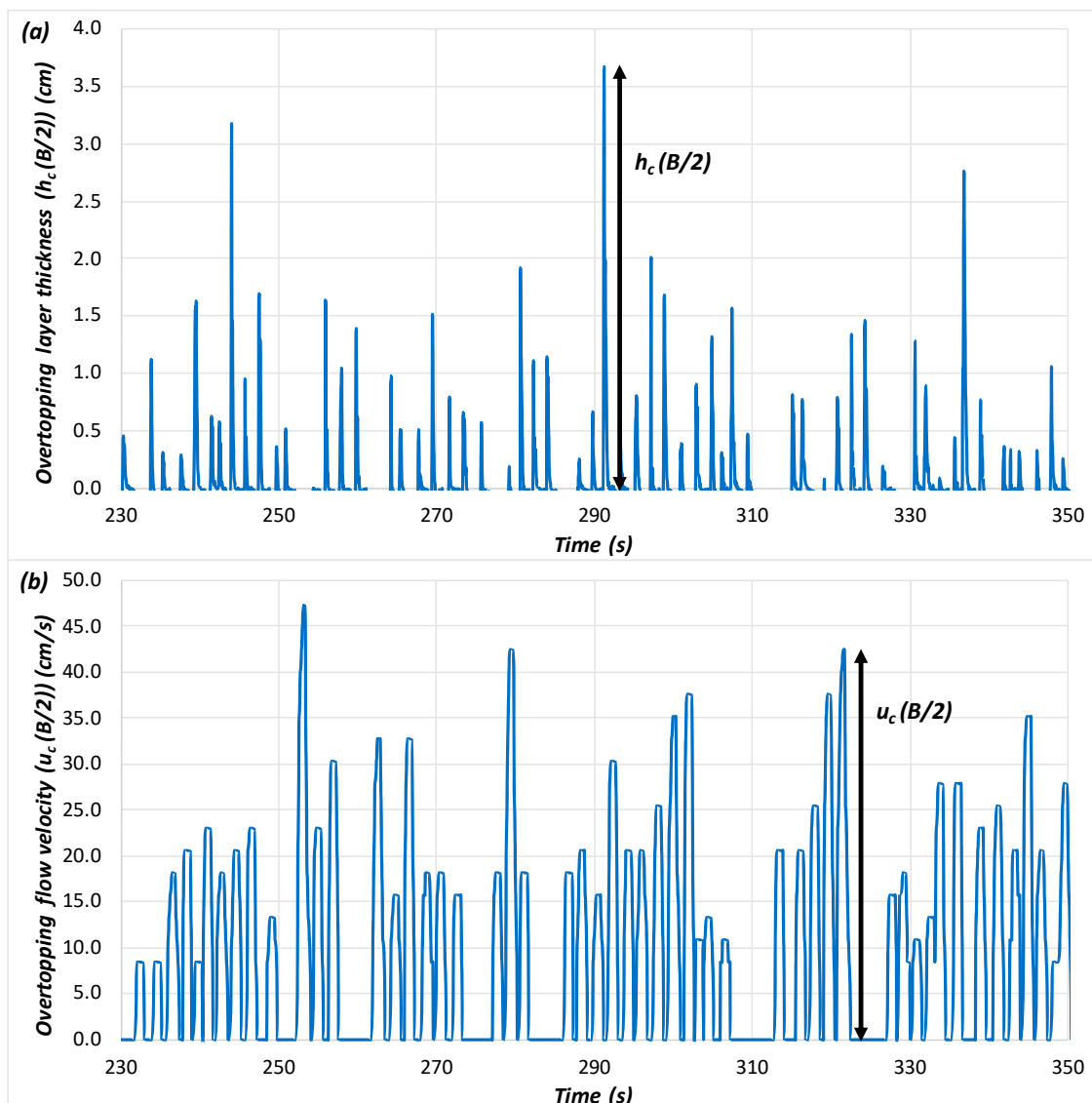
Figure 6. Example of raw records of (**a**) OLT in the middle of the breakwater crest, $h_c(B/2)$, and (**b**) OFV in the middle of the breakwater crest, $u_c(B/2)$.

The OFV was measured in 178 out of 235 physical tests using three miniature propellers on the model crest. Miniature propellers were installed in three different positions: (1) on the seaward edge of the model crest, (2) at the middle of the model crest, and (3) on the leeward edge of the crest. These miniature propellers were able to measure velocities between 0.15 and 3.00 m/s and were able to record instantaneous velocities to a frequency of 20 Hz. From the propeller recordings, the maximum values of the OFV for each overtopping event were obtained similarly to the OLT, as displayed in Figure 6b.

4. Analysis Using Neural Networks

Feedforward neural networks (NNs) are techniques from the artificial intelligence field that can be used to model nonlinear relationships between the input (explanatory) and output (response) variables. Since overtopping is a highly nonlinear problem, NNs have been applied in research and practical applications such as CLASH NN [25]. NNs have also been applied with fewer input variables and smaller datasets, with satisfactory results, to define explicit overtopping formulae [5], to assess the influence of armor placement on hydraulic stability [26], or to identify the most relevant variables to estimate forces on the crown wall [27]. Thus, when the assumption of linear relationships between

variables is not valid, acceptable and reliable results may be obtained when applying NNs rather than conventional methods, such as the case of the influence of bottom slope on the overtopping layer thickness and overtopping flow velocity on mound breakwaters in depth-limited breaking-wave conditions (a highly nonlinear problem).

From the experimental data presented in Section 3, OLT exceeded by 2% of the incoming waves in the middle of the model crest, $h_{c,2\%}(B/2)$ and OFV exceeded by 2% of the incoming waves in the middle of the model crest, $u_{c,2\%}(B/2)$, were determined. Note that the velocity values out of the operational range of the miniature propellers were disregarded. As a result, 57, 30, and 80 values of $u_{c,2\%}(B/2)$ were considered for Cubipod®-1L, rock-2L, and cube-2L models, respectively.

Each armor layer and overtopping variable ($h_{c,2\%}(B/2)$ and $u_{c,2\%}(B/2)$) was studied independently, so the analyses described in the following paragraphs are repeated three times (Cubipod®-1L, rock-2L, and cube-2L) for each overtopping variable ($h_{c,2\%}(B/2)$ and $u_{c,2\%}(B/2)$). The three armor units were studied independently to keep the model as simple as possible. The diagram of this analysis is illustrated in Figure 7.
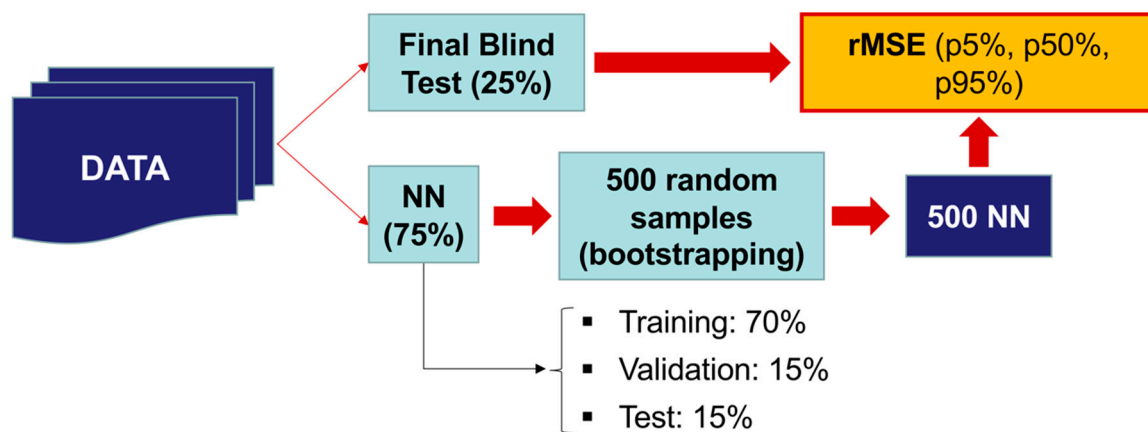
Figure 7. Diagram of the neural network (NN) analysis conducted in this study.

Initially, the data of each armor were divided in two sections: 25% of the data was kept for a final blind test (*FBT*), and 75% of the data was used for the NN training (*T*). The bootstrapping technique is applied to the 75% of the data for training to generate 500 random datasets. This technique consists of the random selection of *N* data from *N* original datasets with a probability of each datum to be selected each time of 1/*N*. Thus, some data were absent in a resample, whereas some data were chosen once or more than once. The 500 random datasets were used to train 500 NNs. The goodness of fit of these NNs was evaluated using *FBT* data with *rMSE*. The average value of *rMSE* and its variability is obtained.

Multi-layer feed-forward NNs with only one hidden layer were used, and a hyperbolic tangent sigmoid transfer function was applied. The NN structure was composed of one input layer of four neurons (N_i), one hidden layer of three neurons (N_h), and one output layer of one neuron (N_o). The number of free parameters of the NN model is given by $P = N_o + N_h (N_i + N_o + 1) = 19$. Overlearning is likely to occur when $P/T \geq 1$, when $P/T = 0.63$ in the worst case. Additionally, an early stopping criterion was applied to prevent overlearning (see MATLAB® [28]), dividing the 75% dataset used for training (*T*) into three sections: training (75% × 70%), validation (75% × 15%), and test (75% × 15%). Data in the training section were used to formally train the NN, updating the biases and weights. Data in the validation section were used to monitor the error after each training step and to stop the training when the error on this subset starts growing (an indication of overlearning). Data in the test section were not used during the training process, but to compare different models as a cross validation. As previously mentioned, every armor layer was studied independently to maintain the simplest NN; in the case of including the three armor layers in one NN, one or several extra input neurons would be needed (e.g., armor element, number of armor layers). In addition, to guarantee a proper NN training, a balance dataset is needed, so the same number of tests from each armor layer

should be used. Therefore, the number of tests used should be limited to the number of cases of the smallest dataset. In other words, only 40 tests would be used (rock-2L), even if 102 and 93 cases are available for Cubipod®-1L and cube-2L, respectively.

As shown in Figure 8, both $h_{c,2\%}(B/2)$ and $u_{c,2\%}(B/2)$ were analyzed as dimensionless variables $(h_{c,2\%}(B/2)/H_s$ and $u_{c,2\%}(B/2)/(H_s/T_{m-1,0}))$. Five input variables were considered as significant to describe OLT and OFV: the significant wave height (H_s), the spectral period ($T_{m-1,0}$), the crest freeboard (R_c), the water depth at the toe of the structure (h_s), and the bottom slope (m). Nevertheless, only four dimensionless variables were considered to feed the NN model (see Figure 8): m, R_c/H_s, $Ir = \tan\alpha/(2\pi H_s/g/T_{m-1,0}^2)$ and h_s/H_s.
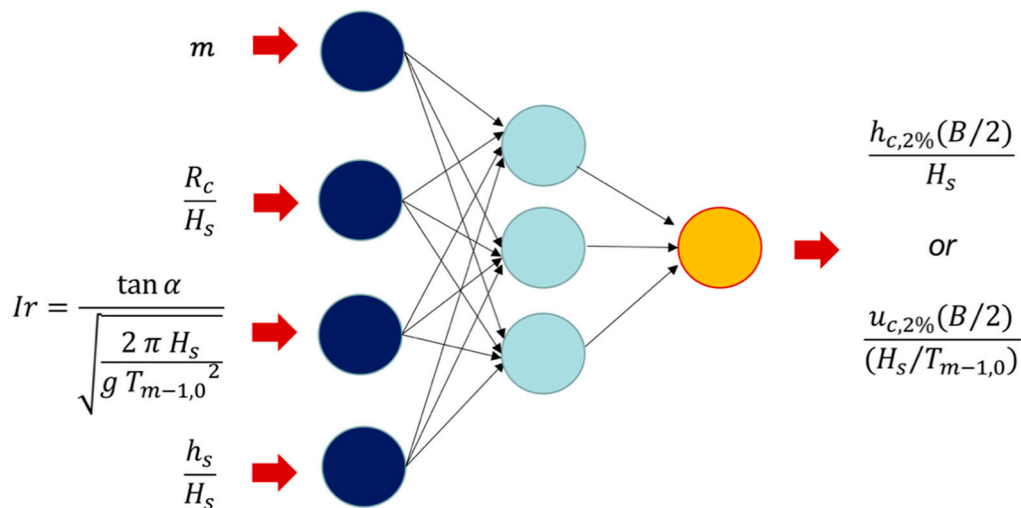
Figure 8. Diagram of the neural networks (NNs) used in this study.

4.1. Optimum Point to Estimate Wave Parameters

The method shown in Figure 7 is repeated seven times for each armor layer and overtopping variable ($7 \times 3 \times 2 = 42$ times), modifying the incident wave height (H_s) given to feed the model. The considered H_s values were H_s estimated at the toe of the structure, H_s estimated at a distance of h_s from the toe of the model, H_s at $2h_s$ from the toe of the model, as so on until $6h_s$ from the breakwater toe.

As a result, the evolution of the percentiles of *rMSE* can be obtained as a function of the distance from the model toe where H_s is calculated. Percentiles 5%, 50%, and 95% were used to characterize *rMSE*. Figure 9 presents the *rMSE* of the NN p50% for $h_{c,2\%}(B/2)$ while Figure 10 shows the results for $u_{c,2\%}(B/2)$. Here, the x-axis represents the distance from the toe to the structure to the point where H_s is calculated as a multiple of h_s, whereas the y-axis presents the median *rMSE* (p50% NN).

The lowest *rMSE* for $h_{c,2\%}(B/2)$ for the three armor layers was obtained around the zone of H_s estimated at a distance of $3h_s$ from the breakwater toe, as shown in Figure 9. In the case of $u_{c,2\%}(B/2)$, no clear tendency was identified for the Cubipod®-1L armor. This may be due to the low number of values for the 2% bottom slope ($N = 13$ for $m = 2\%$, and $N = 44$ for $m = 4\%$). For rock-2L and cube-2L armors, the optimum point to estimate H_s was located between $3h_s$ and $4h_s$ from the toe of the model (see Figure 10). Thus, a distance of $3h_s$ from the model toe was selected as the optimum zone to estimate H_s for the calculation of $h_{c,2\%}(B/2)$ and $u_{c,2\%}(B/2)$. This point was also selected by Herrera et al. [10] to better describe the hydraulic stability of rock-armored rubble mound breakwaters in depth-limited wave conditions. This distance approximately corresponds to the distance of $5H_s$ proposed by Goda [29] and recommended by Melby [30] to determine wave parameters, when considering H_s in breaking wave conditions for vertical breakwaters.
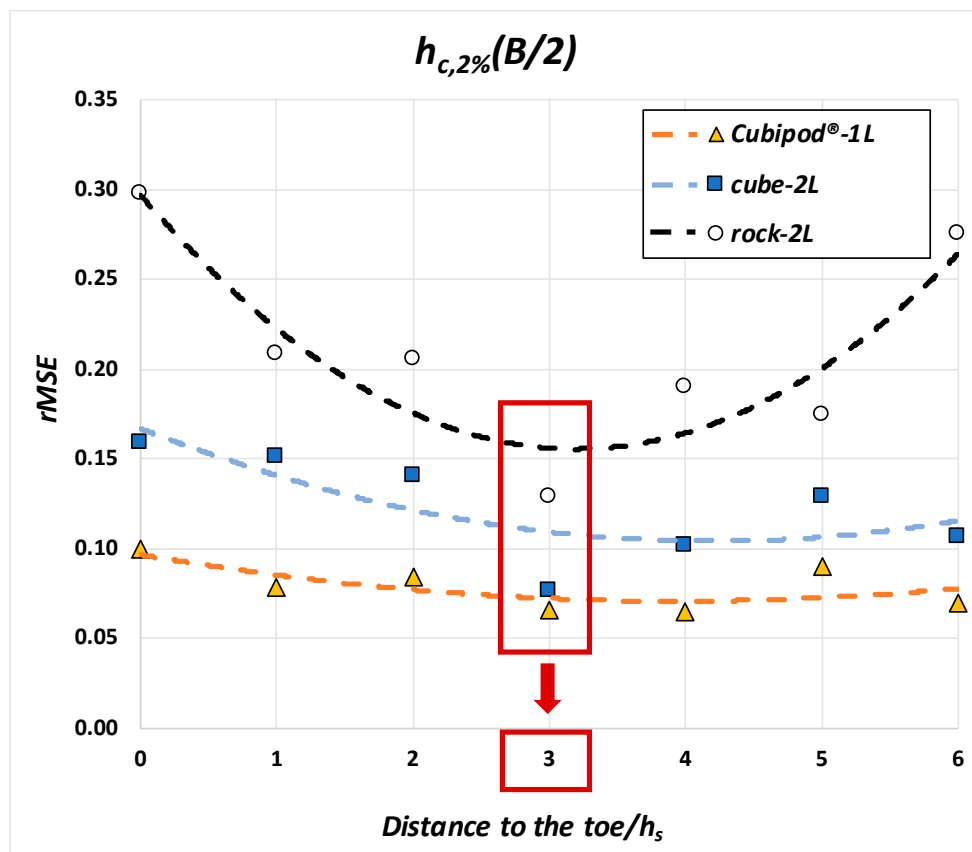
Figure 9. Median relative mean squared error, *rMSE*, (p50% NN) of $h_{c,2\%}(B/2)$ as a function of the relative distance to the structure toe.
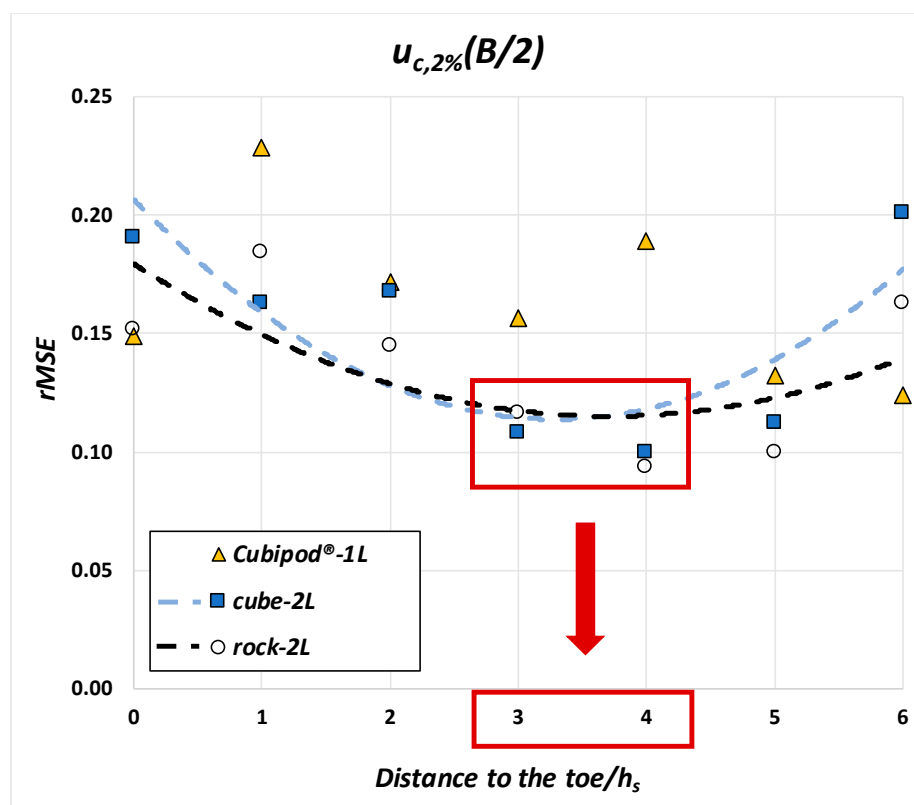

Figure 10. Median *rMSE* (p50% NN) of $u_{c,2\%}(B/2)$ as a function of the relative distance to the structure toe.

4.2. Influence of the Bottom Slope on OLT and OFV

In the previous section, the optimum zone to estimate H_s for the calculation of $h_{c,2\%}(B/2)$ and $u_{c,2\%}(B/2)$ was identified at a distance of $3h_s$ from the model toe. Here, the influence of bottom slope on $h_{c,2\%}(B/2)$ and $u_{c,2\%}(B/2)$ is assessed. To this end, wave conditions were considered in the wave generation zone ($H_{s,g}$ and Ir_g), and they were propagated along the wave flume using the SwanOne model [24] up to a distance of $3h_s$ from the structure toe. Five numerical flumes (see Figure 11) were considered in this propagation, and the gradient of their bottom slope varied within the tested range ($m = 2.0\%$, 2.5%, 3.0%, 3.5%, and 4.0%).
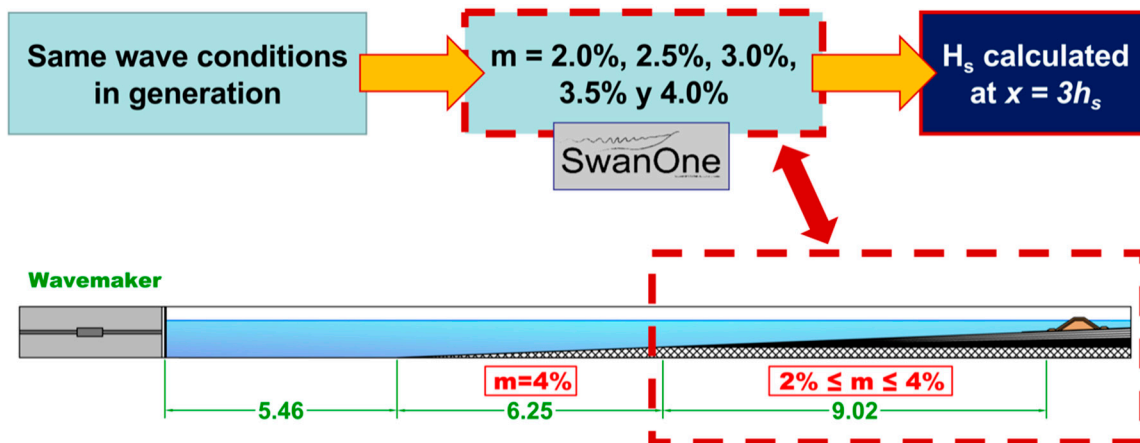
Figure 11. Scheme of the numerical flumes considered for wave propagation using SwanOne.

Using the wave characteristics obtained from the propagation, simulations were conducted using NN p50%. Thus, $h_{c,2\%}(B/2)$ and $u_{c,2\%}(B/2)$ were obtained for five different bottom slopes and the same wave conditions in the wave generation zone. Figure 12 shows the cross-validation of NNs p50% with the final blind test data. The agreement between p50% NNs and the final blind-test data was very good ($0.937 \le r \le 0.971$; $0.066 \le rMSE \le 0.129$).
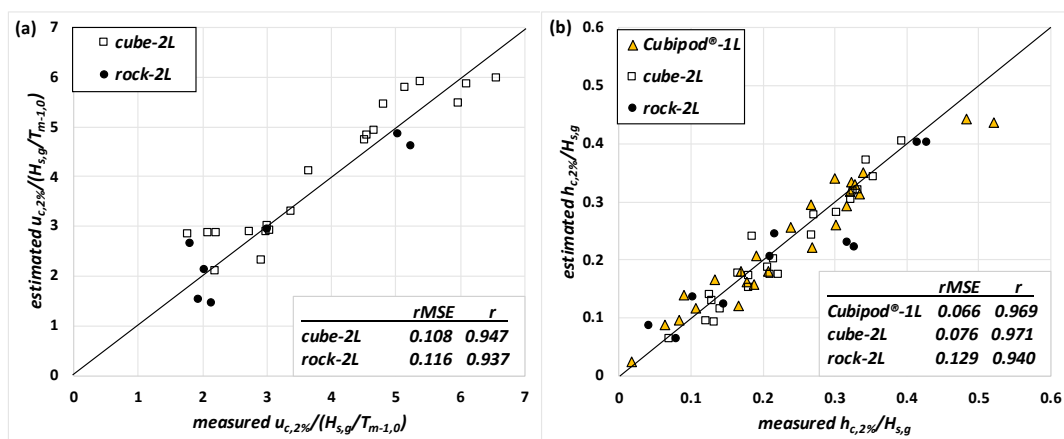

Figure 12. Comparison between measured and estimated blind test data using NN p50% for (**a**) dimensionless $u_{c,2\%}$, and (**b**) dimensionless $h_{c,2\%}$.

Figure 13 illustrates the evolution of $h_{c,2\%}(B/2)$ as a function of m for different wave conditions and the three armor layers (Cubipod®-1L, cube-2L, and rock-2L). $h_{c,2\%}(B/2)$ decreased for increasing values of m.
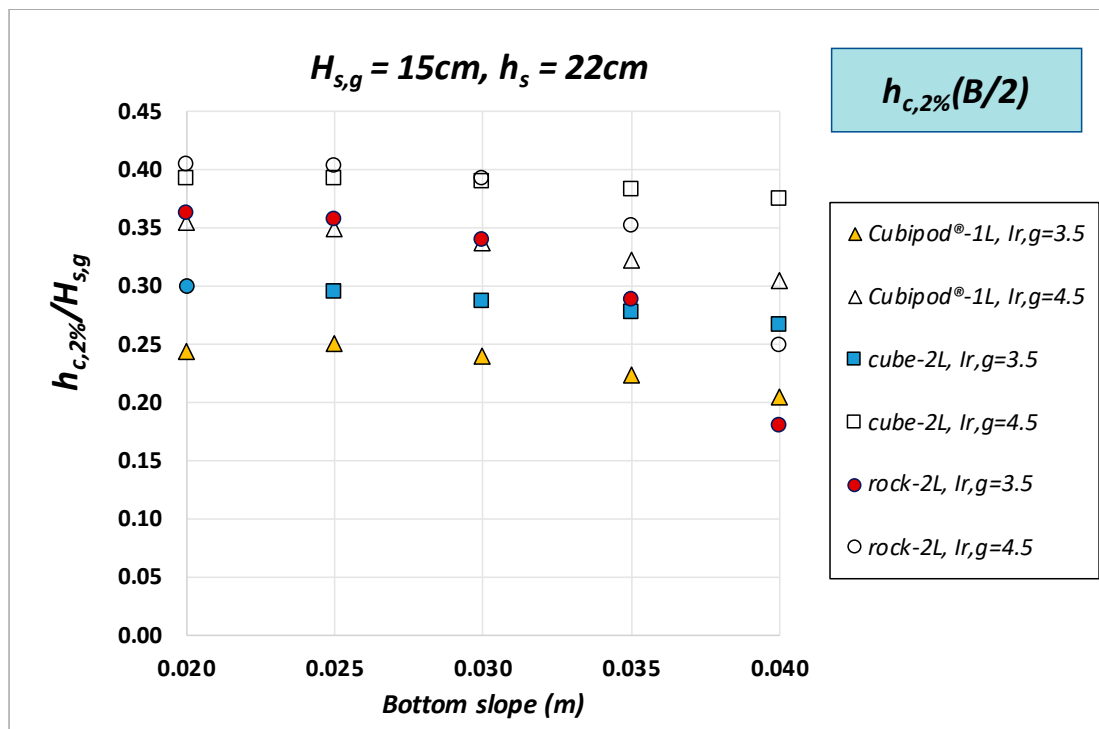
Figure 13. Influence of the bottom slope (*m*) on OLT exceeded by 2% of the incoming waves ($h_{c,2\%}(B/2)$).

Figure 14 shows the progression of $u_{c,2\%}(B/2)$ for cube and rock armors when varying *m* for different wave conditions and two of the three studied armor layers. $u_{c,2\%}(B/2)$ slightly increased with increasing values of *m*.
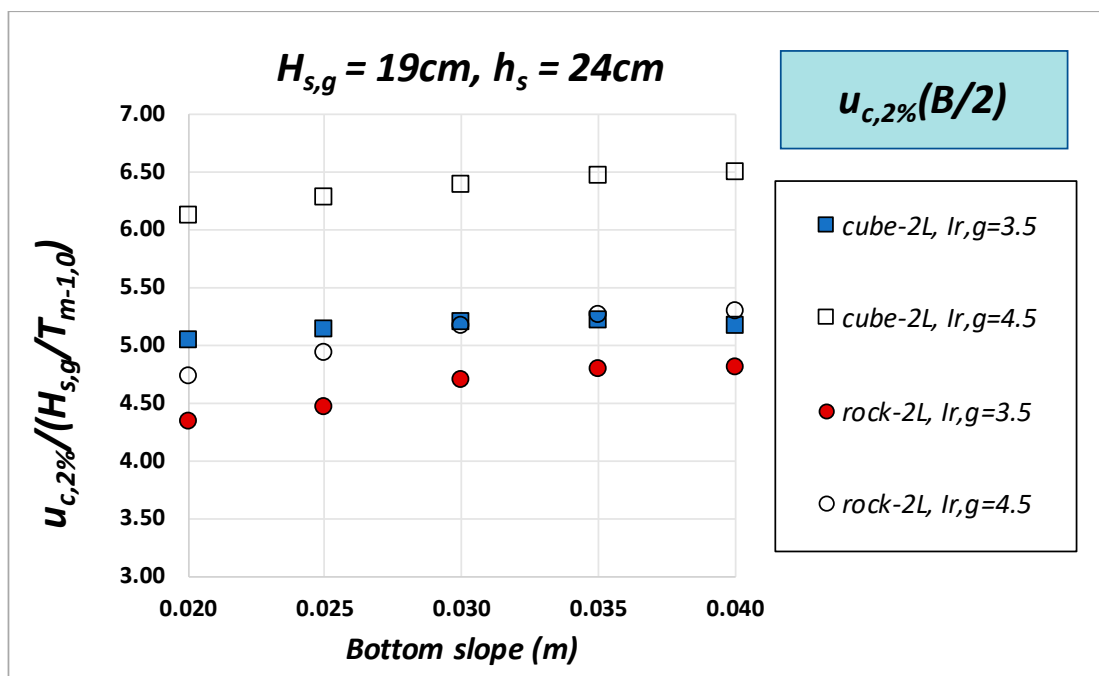

Figure 14. Influence of the bottom slope (*m*) on OFV exceeded by 2% of the incoming waves ($u_{c,2\%}(B/2)$).

5. Conclusions

Overtopping is an increasing risk on coastal structures because of the rising sea levels caused by climate change and social demands to reduce the visual impacts. The safety of pedestrians is a relevant issue during recreational activities on the breakwater crest (e.g., fishing and photography). In order to assess pedestrians' risk, the overtopping layer thickness (OLT) and the overtopping flow velocity (OFV) have been proposed as significant variables.

Few studies are focused on OLT and OFV estimation on coastal structures. These studies only considered variables related to geometry and wave conditions for OLT and OFV calculation. However, most of the mound breakwaters are built in the surf zone, and the bottom slope is an important factor in depth-limited breaking-wave conditions.

In this study, 235 2D physical tests were conducted at the LPC-UPV wave flume with two bottom slopes (m = 2% and m = 4%) and models of mound breakwaters with a single-layer Cubipod® armor, a double-layer rock armor, and a double-layer randomly placed cube armor. A total of 178 tests measured both OLT and OFV, while an additional 57 tests only measured OLT. OLT was measured using a capacitance wave gauge, while OFV was measured using miniature propellers.

Using neural networks (NNs) and bootstrapping techniques, the optimum point to estimate the significant wave height (H_s) to calculate the OLT exceeded by 2% of incoming waves ($h_{c,2\%}(B/2)$) and the OFV exceeded by 2% of incoming waves ($u_{c,2\%}(B/2)$) was studied for each armor. A distance of $3h_s$ from the breakwater toe was determined as the optimum zone to estimate H_s for the calculation of $h_{c,2\%}(B/2)$ and $u_{c,2\%}(B/2)$.

In order to analyze the influence of m on $h_{c,2\%}(B/2)$ and $u_{c,2\%}(B/2)$, fixed wave conditions in the wave generation zone were propagated along five numerical wave flumes with different bottom slopes (m = 2.0%, 2.5%, 3.0%, 3.5%, and 4.0%) using the SwanOne software [24] up to a distance of $3h_s$ from the model toe. Using the median *rMSE* NNs (p50% NN), it is observed how $h_{c,2\%}(B/2)$ decreases and $u_{c,2\%}(B/2)$ slightly increases as the gradient of the bottom slope increases.

References

1. Franco, L.; de Gerloni, M.; van der Meer, J.W. Wave overtopping on vertical and composite breakwaters. In Proceedings of the 24th International Conference on Coastal Engineering, Kobe, Japan, 23–28 October 1994; ASCE: Reston, VA, USA, 1994; pp. 1030–1044.
2. Bae, H.U.; Yun, K.M.; Yoon, J.Y.; Lim, N.H. Human Stability with respect to overtopping flow on the breakwater. *Int. J. Appl. Eng. Res.* **2016**, *11*, 111–119.
3. Sandoval, C.; Bruce, T. Wave overtopping hazard to pedestrians: Video evidence from real accidents. In Proceedings of the Coasts, Marine Structures and Breakwaters 2017, Liverpool, UK, 5–7 September 2017; ICE Publishing: Scotland, UK, 2017; pp. 501–512.
4. EurOtop. *Manual on Wave Overtopping of Sea Defences and Related Structures*; An overtopping manual largely based on European research, but for worldwide application. Van der Meer, J.W., Allsop, N.W.H., Bruce, T., De Rouck, J., Kortenhaus, A., Pullen, T., Schüttrumpf, H., Troch, P., Zanuttigh, B., Eds.; EurOtop, 2018. Available online: www.overtopping-manual.com (accessed on 15 March 2019).

5. Molines, J.; Medina, J.R. Explicit wave overtopping formula for mound breakwaters with crown walls using CLASH neural network derived-data. *J. Waterw. Port Coast. Ocean Eng.* **2015**, *142*, 04015024. [CrossRef]

6. Nørgaard, J.Q.H.; Lykke-Andersen, T.; Burcharth, H.F. Distribution of individual wave overtopping volumes in shallow water wave conditions. *Coast. Eng.* **2014**, *83*, 15–23. [CrossRef]

7. Molines, J.; Herrera, M.P.; Gómez-Martín, M.E.; Medina, J.R. Distribution of individual wave overtopping volumes on mound breakwaters. *Coast. Eng.* **2019**, *149*, 15–27. [CrossRef]

8. Schüttrumpf, H.; van Gent, M. Wave overtopping at seadikes. In Proceedings of the Coastal Structures, Portland, OR, USA, 26–30 August 2003; ASCE: Reston, VA, USA, 2003; pp. 431–443.

9. Mares-Nasarre, P.; Argente, G.; Gómez-Martín, M.E.; Medina, J.R. Overtopping layer thickness and overtopping flow velocity on mound breakwaters. *Coast. Eng.* **2019**, *154*, 103561. [CrossRef]

10. Herrera, M.P.; Gómez-Martín, M.E.; Medina, J.R. Hydraulic stability of rock armors in breaking wave conditions. *Coast. Eng.* **2017**, *127*, 55–67. [CrossRef]

11. Van Gent, M. Wave overtopping events at dikes. In Proceedings of the 28th International Conference on Coastal Engineering, Cardiff, UK, 7–12 July 2002; World Scientific: Singapore, 2002; pp. 2203–2215. [CrossRef]

12. Schüttrumpf, H.; Möller, J.; Oumeraci, H. Overtopping flow parameters on the inner slope of seadikes. In Proceedings of the 28th International Conference on Coastal Engineering, Cardiff, UK, 7–12 July 2002; World Scientific: Singapore, 2002; pp. 2116–2127. [CrossRef]

13. Van Gent, M. Wave runup on dikes with shallow foreshores. *J. Waterw. Port Coast. Ocean Eng.* **2001**, *127*, 254–262. [CrossRef]

14. Van der Meer, J.W.; Hardeman, B.; Steendam, G.; Schïuttrumpf, H.; Verheij, H. Flow depths and velocities at crest and landward slope of a dike, in theory and with the wave overtopping simulator. In Proceedings of the 32nd International Conference on Coastal Engineering, Shanghai, China, 30 June–5 July 2010; World Scientific: Singapore, 2010; p. 2728. [CrossRef]

15. Lorke, S.; Scheres, B.; Schüttrumpf, H.; Bornschein, A.; Pohl, R. Physical model tests on wave overtopping and flow processes on dike crests influenced by wave-current interaction. In Proceedings of the 33rd International Conference on Coastal Engineering, Santander, Spain, 1–6 July 2012; World Scientific: Singapore, 2012; p. 1770. [CrossRef]

16. Mansard, R.P.D.; Funke, E.R. The measurement of incident and reflected spectra using a least squares method. In Proceedings of the 17th International Conference on Coastal Engineering, Sydney, Australia, 23–28 March 1980; ASCE: Reston, VA, USA, 1980; pp. 100–108.

17. Herrera, M.P.; Medina, J.R. Toe berm design for very shallow waters. *Coast. Eng.* **2015**, *103*, 67–77. [CrossRef]

18. Gómez-Martín, M.E.; Medina, J.R. Heterogeneous packing and hydraulic stability of cube and Cubipod® armor units. *J. Waterw. Port Coast. Ocean Eng.* **2014**, *140*, 100–108. [CrossRef]

19. Argente, G.; Gómez-Martín, M.E.; Medina, J.R. Hydraulic Stability of the Armor Layer of Overtopped Breakwaters. *J. Mar. Sci. Eng.* **2018**, *6*, 143. [CrossRef]

20. Gómez-Martín, M.E.; Herrera, M.P.; Gónzalez-Escriva, J.A.; Medina, J.R. Cubipod® Armor Design in Depth-Limited Regular Wave-Breaking Conditions. *J. Mar. Sci. Eng.* **2018**, *6*, 150. [CrossRef]

21. Figueres, M.; Medina, J.R. Estimating incident and reflected waves using a fully nonlinear wave model. In Proceedings of the 29th International Conference on Coastal Engineering, Lisbon, Portugal, 19–24 September 2004; World Scientific: Singapore, 2004; pp. 594–603. [CrossRef]

22. Battjes, J.A.; Groenendijk, H.W. Wave height distributions on shallow foreshores. *Coast. Eng.* **2000**, *40*, 161–182. [CrossRef]

23. Victor, L.; van der Meer, J.W.; Troch, P. Probability distribution of individual wave overtopping volumes for smooth impermeable steep slopes with low crest freeboards. *Coast. Eng.* **2012**, *64*, 87–101. [CrossRef]

24. Verhagen, H.J.; Van Vledder, G.; Eslami Arab, S. A practical method for design of coastal structures in shallow water. In Proceedings of the 31st International Conference on Coastal Engineering, Hamburg, Germany, 31 August–5 September 2008; World Scientific: Singapore, 2008; pp. 2912–2922. [CrossRef]

25. Van Gent, M.R.A.; Van den Boogaard, H.F.P.; Pozueta, B.; Medina, J.R. Neural network modelling of wave overtopping at coastal structures. *Coast. Eng.* **2007**, *54*, 586–593. [CrossRef]

26. Herrera, M.P.; Hoyos, A.; Molines, J.; Medina, J.R. Influence of placement technique on double-layer cube armor stability of breakwaters constructed on steep foreshores. In Proceedings of the 36th IAHR World Congress, The Hague, The Netherlands, 28 June–3 July 2015.

27.   Molines, J.; Herrera, M.P.; Medina, J.R. Estimations of wave forces on crown walls based on wave overtopping rates. *Coast. Eng.* **2018**, *132*, 50–62. [CrossRef]

28.   *MATLAB® 2015a*; The MathWorks Inc.: Natick, MA, USA, 2015.

29.   Goda, Y. *Random Seas and Design of Maritime Structures*; University of Tokyo Press: Tokyo, Japan, 1985.

30.   Melby, J.A. *Damage Progression on Rubble Mound Breakwaters*; Technical Report CHL-99-17; U.S. Army Engineer Research and Development Center: Vicksburg, MS, USA, 1999; Also Ph.D. Thesis, University of Delaware, Newark, DE, USA, 1999.